Motion of guiding center drift atoms in the electric and magnetic field of a Penning trap

S. G. Kuzmin and T. M. O'Neil
Department of Physics, University of California at San Diego, La Jolla, California 92093

(Received 2 July 2004; accepted 22 September 2004; published online 23 November 2004)

The ApparaTus for High precision Experiment on Neutral Antimatter and antihydrogen TRAP collaborations have produced antihydrogen atoms by recombination in a cryogenic antiproton-positron plasma. This paper discusses the motion of the weakly bound atoms in the electric and magnetic field of the plasma and trap. The effective electric field in the moving frame of the atom polarizes the atom, and then gradients in the field exert a force on the atom. An approximate equation of motion for the atom center of mass is obtained by averaging over the rapid internal dynamics of the atom. The only remnant of the atom internal dynamics that enters this equation is the polarizability for the atom. This coefficient is evaluated for the weakly bound and strongly magnetized (guiding center drift) atoms understood to be produced in the antihydrogen experiments. Application of the approximate equation of motion shows that the atoms can be trapped radially in the large space charge field near the edge of the positron column. Also, an example is presented for which there is full three-dimensional trapping, not just radial trapping. Even untrapped atoms follow curved trajectories, and such trajectories are discussed for the important class of atoms that reach a field ionization diagnostic. Finally, the critical field for ionization is determined as an upper bound on the range of applicability of the theory. © *2005 American Institute of Physics*. [DOI: 10.1063/1.1818140]

I. INTRODUCTION

The ATHENA (ApparaTus for High precision Experiment on Neutral Antimatter) and ATRAP (antihydrogen TRAP) collaborations at CERN (European Organization for Nuclear Research) have reported the production of cold antihydrogen atoms.[1,2] The atoms result from recombination when cold antiprotons are added to a cryogenic positron plasma in a Penning trap configuration. The ATRAP collaboration measured binding energies in the range of meV.[3]

Here we discuss the motion of these weakly bound atoms in the magnetic and electric field of the trap. Because the binding is so weak, even a modest electric field produces a significant polarization of an atom. A gradient in the field then exerts a force on the atom, causing acceleration. Typically, the atom is moving across the magnetic field, and it is the effective electric field in the moving frame of the atom that causes the polarization and the acceleration. In the laboratory frame, both electric and magnetic forces must be taken into account.

In the experiments, the magnetic field is nearly uniform and the electric field varies by only a small amount over the dimensions of the atom. Also, the time scale for the internal dynamics of the atom is short compared to the time scale for the atom to move a significant distance. Taking advantage of these orderings, we obtain an approximate equation of motion for the atom center of mass. The only remnant of the atom internal dynamics that enters the equation of motion is the polarizability. The approximate equation of motion provides a substantial simplification because it averages over the rapid internal dynamics of the atom.

An interesting implication of the equation of motion is that a weakly bound atom can be trapped radially in the large electric field region near the edge of a long cylindrical positron column. The reason for the trapping is easy to understand physically. For a uniform density unneutralized column of positrons, the radial space charge field increases linearly with radius inside the column and falls off inversely with radius outside the column. Thus, there is a region of large field near the plasma edge, and polarizable material (the atom) is attracted to a region of maximum field. Also, we will see that certain equilibrium configurations for the positron plasma make possible full three-dimensional trapping, not just radial trapping.

We will find that the polarization forces create a potential well of approximate depth αE^2, where α is the polarizability of the atom and E is the electric field strength. In Gaussian units, the polarizability has the dimensions length cubed, and the polarizability for an atom of size r_a is of order $\alpha \sim r_a^3$. Since the binding energy for an atom is of order e^2/r_a, the depth of the well scales inversely with the cube of the binding energy. Thus, the effects discussed here are more pronounced for weakly bound atoms. Of course, a weakly bound atom suffers field ionization from a relatively weak field. The critical field for ionization is approximately $E \sim e/r_a^2$. Using this field strength as an upper bound for E shows that the maximum well depth is the binding energy of the atom:

$$\alpha E^2 = (\alpha/r_a^3) r_a^3 \left(\frac{E}{e/r_a^2}\right)^2 \left(\frac{e}{r_a^2}\right)^2 \lesssim \frac{e^2}{r_a}. \tag{1}$$

For the example discussed in the last paragraph, trapping is possible only when the atom binding energy is larger than the kinetic energy of the atom center of mass.

The ATRAP collaboration uses field ionization as a diagnostic, and the ionization region is some distance from the plasma. As a second application of the approximate equation of motion, we determine trajectories followed by weakly bound atoms in moving from the recombination region (inside the positron plasma) to the field ionization region. Depending on the parameters, a straight line orbit may or may not be a good approximation. We will see that the polarization forces produce a significant deflection of the atom when the binding energy is larger than the center of mass kinetic energy. Knowledge of the trajectories is an important input to estimates of antihydrogen production rates based on solid angle considerations.

The analysis divides naturally into two parts: the derivation of the equation of motion and the calculation of the polarizability. In Sec. II, we derive an approximate equation of motion for the expectation value of the atom center of mass coordinates, $\langle \mathbf{R}_{\rm cm}\rangle(t) \equiv \langle \Psi | \mathbf{R}_{\rm cm} | \Psi \rangle$. The derivation of the equation of motion depends on the spatial and temporal orderings mentioned above but otherwise is general. On the other hand, determination of the polarizability requires a more detailed specification of the internal dynamics for the atom.

In Sec. III, we evaluate the polarizability for the special case of guiding center drift atoms.[4] As discussed in recent literature,[5,6] these weakly bound and strongly magnetized atoms are thought to be produced in the antihydrogen experiments. For these atoms, the cyclotron frequency for the positron is much larger than the other dynamical frequencies and the cyclotron radius is much smaller than the separation between the positron and antiproton. Under these circumstances, the rapid cyclotron motion can be averaged out and the positron dynamics treated by guiding center drift theory. The dynamics is quasiclassical, since the binding energy is much smaller than the Rydberg energy (four orders of magnitude smaller for the meV binding energies measured in the ATRAP experiments). Fortunately, the dynamics for guiding center atoms is integrable, and the polarizability can be evaluated with perturbation theory.

Section IV contains applications of the approximate equation of motion. As a first application, we demonstrate the radial trapping of weakly bound atoms in the large space charge field of a long positron column. The geometry and field strengths used are characteristic of the ATHENA experiments. Orbits from the approximate equation of motion are shown to be in good agreement with those from lengthy numerical solutions of the coupled positron-antiproton equations of motion. These latter solutions involve over a million cycles of the internal atom dynamics. The comparison demonstrates the fidelity of the approximate equation of motion and also the substantial simplification it provides in averaging out the rapid internal dynamics.

Certain equilibrium configurations for the positron plasma make possible full three dimensional trapping, not just radial trapping. As a simple example, we consider a spherical plasma in a quadratic trap potential. The self-consistent fields for this equilibrium are evaluated in the Appendix, and in Sec. IV the fields are shown to produce full three dimensional trapping. The potential energy function associated with the polarization forces is a three-dimensional potential well, and atoms with sufficiently small kinetic energy simply cannot escape.

Finally, the approximate equation of motion is used to obtain the curved trajectories followed by weakly bound atoms in moving from the plasma to a field ionization region. Here we use field strengths and geometry characteristic of ATRAP.

For the special case of a purely radial space charge field, the approximate equation of motion was obtained previously.[7] The derivation here is more general in that it allows all three components of the electric field. Also, the derivation here is not based on classical mechanics and the guiding center drift approximation. This specialization is used here only to obtain the polarizability, not in the derivation of the approximate equation of motion. The present discussion of the polarizability tensor is more complete than in Ref. 7 and includes a discussion of field ionization. Also, the demonstration of three dimensional trapping and the determination of trajectories for atoms moving from the plasma to the field ionization region are new.

II. APPROXIMATE EQUATION OF MOTION

We consider a positron (particle 1) and an antiproton (particle 2), although the results apply equally to an electron and a singly ionized ion. The mass ratio m_1/m_2 is assumed to be small, but is not specified to a specific value. The two particles interact electrostatically and move in the uniform magnetic field $\mathbf{B}=\hat{z}B$ and the spatially varying electric field $\mathbf{E}=-\boldsymbol{\nabla}\phi$. For the choice of vector potential $\mathbf{A}=Bx\hat{y}$, the Hamiltonian operator is given by

$$H = \frac{p_{z1}^2}{2m_1} + \frac{p_{x1}^2}{2m_1} + \frac{\left(p_{y1} - \dfrac{eB}{c}x_1\right)^2}{2m_1} + \frac{p_{z2}^2}{2m_2} + \frac{p_{x2}^2}{2m_2} + \frac{\left(p_{y2} + \dfrac{eB}{c}x_2\right)^2}{2m_2} - \frac{e^2}{\sqrt{(x_1-x_2)^2+(y_1-y_2)^2+(z_1-z_2)^2}} + e\phi(x_1,y_1,z_1) - e\phi(x_2,y_2,z_2). \tag{2}$$

The effect of spin has been neglected, since the magnetic field is uniform and the spin-field interaction does not couple the spin and orbital dynamics. The usual spin-orbit interaction, which is smaller than the electrostatic interaction by order $(v/c)^2$, is very small for the small binding energies (and small velocities) considered here.

It is useful to introduce relative coordinates through the transformation

$$x = x_1 - x_2, \quad p_x = \frac{m_2 p_{x1} - m_1 p_{x2}}{m_1 + m_2},$$

$$y = y_1 - y_2, \quad p_y = \frac{m_2\left(p_{y1} - \dfrac{eB}{c}x_2\right) - m_1\left(p_{y2} + \dfrac{eB}{c}x_1\right)}{m_1 + m_2},$$

$$z = z_1 - z_2, \quad p_z = \frac{m_2 p_{z1} - m_1 p_{z2}}{m_1 + m_2},$$

$$X = \frac{m_1 x_1 + m_2 x_2}{m_1 + m_2} + \frac{c}{eB}(p_{y1} + p_{y2}),$$

$$P_X = p_{x1} + p_{x2} - \frac{eB}{c}(y_1 - y_2),$$

$$Y = \frac{(2m_2 + m_1)y_2 - m_2 y_1}{m_1 + m_2} + \frac{c}{eB}(p_{x1} + p_{x2}), P_Y = p_{y1} + p_{y2},$$

$$Z = \frac{m_1 z_1 + m_2 z_2}{m_1 + m_2}, \quad P_Z = p_{z1} + p_{z2}. \tag{3}$$

Classically, this is a canonical transformation, as can be verified by observing that the Poisson brackets for the new coordinates and momenta have the canonical values (i.e., $[Q_i, P_j] = \delta_{ij}$). Quantum mechanically, the commutators for the new operations have the canonical values (i.e., $[Q_r, P_s] = \delta_{rs} i\hbar$).

The vector $\mathbf{r} = (x, y, z)$ is the relative coordinate between the positron and antiproton. The momentum P_Z is the total (or center of mass) momentum along the magnetic field. The transverse components (P_X, P_Y) are often called pseudomenta.[8] P_Y is the sum of the y components of the canonical momentum for the two particles; P_X is the corresponding sum that would be obtained for the x components using a different choice of vector potential (i.e., $\mathbf{A}' = -By\hat{x}$). The two choices ($\mathbf{A} = Bx\hat{y}$ and $\mathbf{A}' = -By\hat{x}$) are related by a gauge transformation and both produce the given magnetic field (i.e., $\nabla \times \mathbf{A} = \nabla \times \mathbf{A}' = \hat{z}B$). We will see that $\mathbf{P} = (P_X, P_Y, P_Z)$ are constants of the motion for the special case of a spatially uniform electric field.

For future convenience, we note that the antiproton and positron coordinates are given by

$$\mathbf{r}_2 = \left(X - \frac{c}{eB} P_Y - \frac{m_1 x}{m_1 + m_2}, Y - \frac{c}{eB} P_X - \frac{m_1 y}{m_1 + m_2}, Z - \frac{m_1 z}{m_1 + m_2} \right), \tag{4}$$

$$\mathbf{r}_1 = \mathbf{r}_2 + \mathbf{r}. \tag{5}$$

Likewise, the center of mass coordinates are given by

$$\mathbf{R}_{\rm cm} = \frac{m_1 \mathbf{r}_1 + m_2 \mathbf{r}_2}{m_1 + m_2} = \left(X - \frac{c}{eB} P_Y, Y - \frac{c}{eB} P_X, Z \right). \tag{6}$$

In terms of the new operators, the Hamiltonian is given by

$$H = \frac{|\mathbf{P}|^2}{2M} - \frac{eB}{MC}(P_Y x - P_X y) + \frac{M\Omega_{\rm CM}^2}{2}(x^2 + y^2) + \frac{p_x^2}{2\mu} + \frac{\left(p_y - \sqrt{1 - \frac{4\mu}{M}\frac{eB}{c} x} \right)^2}{2\mu} + \frac{p_z^2}{2\mu} - \frac{e^2}{\sqrt{x^2 + y^2 + z^2}} + e\phi(\mathbf{r}_1) - e\phi(\mathbf{r}_2), \tag{7}$$

where $M = m_1 + m_2$ and $\mu = m_1 m_2/(m_1 + m_2)$ are the total and reduced mass, $\Omega_{\rm CM} \equiv eB/MC$ is the cyclotron frequency for the total mass, and $\mathbf{r}_2$ and $\mathbf{r}_1$ have been introduced as shorthand for the variables in relations (4) and (5).

Let $\langle \mathbf{P} \rangle \equiv \langle \Psi | \mathbf{P} | \Psi \rangle$ be the expectation value of the total momentum. The rate of change of this quantity is given by

$$\frac{d}{dt}\langle \mathbf{P} \rangle = \langle \Psi | \frac{1}{i\hbar}[\mathbf{P}, H] | \Psi \rangle. \tag{8}$$

Using $\mathbf{P} = (\hbar/i)(\partial/\partial X, \partial/\partial Y, \partial/\partial Z)$ to evaluate the commutator $[\mathbf{P}, H]$ yields the result

$$\frac{d\langle \mathbf{P} \rangle}{dt} = \langle \Psi | [e\mathbf{E}(\mathbf{r}_1) - e\mathbf{E}(\mathbf{r}_2)] | \Psi \rangle, \tag{9}$$

where the electric field $\mathbf{E} = -\nabla\phi$, has been introduced. As anticipated, $\mathbf{P}$ is a constant of the motion for the case of a spatially uniform electric field.

We assume that the spatial gradient in the field is small and work only to first order in the gradient. Let $\ell \sim |\mathbf{E}|/|\nabla E|$ be the scale length of the field and r_a be the size of the atom. Formally, the wave function $|\Psi\rangle$ is negligibly small for $r = |\mathbf{r}_1 - \mathbf{r}_2|$ larger than r_a. We assume that $r_a \ll \ell$, and work only to first order in the small parameter $r_a/\ell \ll 1$. To this order, Eq. (9) can be rewritten as

$$\frac{d\langle \mathbf{P} \rangle}{dt} \simeq \langle \Psi | [e\mathbf{r} \cdot \nabla \mathbf{E}(\langle \mathbf{R}_{\rm cm} \rangle)] | \Psi \rangle, \tag{10}$$

where $\langle \mathbf{R}_{\rm cm} \rangle \equiv \langle \Psi | \mathbf{R}_{\rm cm} | \Psi \rangle$ is the expectation value of the center of mass position operator [see Eq. (6)]. In terms of the expectation value $\langle \mathbf{r} \rangle \equiv \langle \Phi | \mathbf{r} | \Psi \rangle$, Eq. (10) takes simple form

$$\frac{d\langle \mathbf{P} \rangle}{dt} \simeq e\langle \mathbf{r} \rangle \cdot \nabla \mathbf{E}(\langle \mathbf{R}_{\rm cm} \rangle). \tag{11}$$

Likewise, the rate of change of $\langle \mathbf{R}_{\rm cm} \rangle$ is given by

$$\frac{d\langle \mathbf{R}_{\rm cm} \rangle}{dt} = \langle \Psi | \frac{1}{i\hbar}[\mathbf{R}_{\rm cm}, H] | \Psi \rangle = \frac{\langle \mathbf{P} \rangle}{M} + \frac{e\langle \mathbf{r} \rangle}{MC} \times \mathbf{B}, \tag{12}$$

where use has been made of definition (6), Hamiltonian (7), and the basic commutator relations. Taking the time derivative of Eq. (12) and using Eq. (11) to replace $d\langle \mathbf{P} \rangle/dt$ yields the result

$$M\frac{d^2\langle \mathbf{R}_{\rm cm} \rangle}{dt^2} = \mathbf{d} \cdot \nabla \mathbf{E}(\langle \mathbf{R}_{\rm cm} \rangle) + \frac{1}{c}\frac{d}{dt}\mathbf{d} \times \mathbf{B}, \tag{13}$$

where $\mathbf{d} \equiv e\langle \mathbf{r} \rangle$ is the dipole moment of the atom.

The next step is to find an expression for $\mathbf{d}$ in terms of fields and the center of mass velocity [i.e., $\mathbf{E}(\langle \mathbf{R}_{\rm cm} \rangle)$, $\mathbf{B}$, and $d\langle \mathbf{R}_{\rm cm} \rangle/dt$]. Equation (13) will then be a proper equation of motion for the evolution of $\langle \mathbf{R}_{\rm cm} \rangle(t)$ in the given fields.

The first term on the right-hand side of Eq. (13) is obviously first order in the spatial gradient of the electric field [i.e., $O(1/\ell)$], and the second term is as well, since d/dt turns out to be first order in the gradient. Thus, in Hamiltonian (7) we set $e\phi(r_1) - e\phi(r_2) = e\mathbf{E} \cdot \mathbf{r}$, where the field $\mathbf{E}$ is independent of $\mathbf{r}$. To zero order in $r_a/\ell \ll 1$, we set $\mathbf{E} = \mathbf{E}(\langle \mathbf{R}_{\rm cm} \rangle)$.

There remains the question of the time dependence in $\mathbf{E}[\langle \mathbf{R}_{cm}\rangle(t)]$. We assume that the time scale for the internal dynamics (relative motion) is short compared to the time for the atom as a whole to move a distance ℓ. This latter time is the time scale on which $\mathbf{E}[\langle \mathbf{R}_{cm}\rangle(t)]$ changes significantly. Thus, we use an adiabatic approximation and neglect the time dependence in $\mathbf{E}[\langle \mathbf{R}_{cm}\rangle(t)]$ when solving for the internal motion (relative motion).

As mentioned earlier, $\mathbf{P}$ is a constant of the motion for a uniform electric field. Thus, in Hamiltonian (7) we replace the operator $\mathbf{P}$ by the constant eigenvalue $\mathbf{P}$ and replace the potential difference $[e\phi(\mathbf{r}_1)-e\phi(\mathbf{r}_2)]$ by $-e\mathbf{E}\cdot\mathbf{r}$ where $\mathbf{E}$ is a constant field. This yields a Hamiltonian for the relative motion

$$H=\frac{p_x^2}{2\mu}+\frac{\left(p_y-\sqrt{1-\frac{4\mu}{M}}\frac{eB}{c}x\right)^2}{2\mu}+\frac{p_z^2}{2\mu}-\frac{e^2}{\sqrt{x^2+y^2+z^2}}+\frac{M}{2}\Omega_{CM}^2(x^2+y^2)-e\boldsymbol{\mathcal{E}}\cdot\mathbf{r}, \tag{14}$$

where

$$\boldsymbol{\mathcal{E}}=\mathbf{E}+\frac{\mathbf{P}\times\mathbf{B}}{MC} \tag{15}$$

is the effective field acting on the atom, and the constant term $P^2/(2M)$ has been dropped from the Hamiltonian.

For the special case $\boldsymbol{\mathcal{E}}=0$, H commutes with the parity operator $\mathcal{P}$. If $\psi_{n_1,n_2,n_3}(\mathbf{r})$ is an eigenfunction of H corresponding to the eigenvalue $\overline{H}_{n_1,n_2,n_3}$, then $\mathcal{P}\psi_{n_1,n_2,n_3}(\mathbf{r})=\psi_{n_1,n_2,n_3}(-\mathbf{r})$ is an eigenfunction for the same eigenvalue. Except for very special cases (e.g., $\mathbf{B}=0$), one expects the energy levels $\overline{H}_{n_1,n_2,n_3}$ to be nondegenerate. Here, the integers (n_1,n_2,n_3) specify the quantum state. For the special case of guiding center drift dynamics, we will identify these integers in the following section. Therefore, $\mathcal{P}\psi_{n_1,n_2,n_3}$ and ψ_{n_1,n_2,n_3} differ only by a constant; further, that constant must be ±1, that is, ψ_{n_1,n_2,n_3} must have even or odd parity. Thus, the dipole moment $\mathbf{d}=e\langle\Psi|\mathbf{r}|\Psi\rangle$ vanishes for $\boldsymbol{\mathcal{E}}=0$.

For sufficiently small $\boldsymbol{\mathcal{E}}$, Taylor expansion suggests the linear relationship $\mathbf{d}=\hat{\alpha}\cdot\boldsymbol{\mathcal{E}}$, where the polarizability matrix is given by

$$\hat{\alpha}=\begin{pmatrix}\alpha_\perp & 0 & 0\\ 0 & \alpha_\perp & 0\\ 0 & 0 & \alpha_z\end{pmatrix}. \tag{16}$$

Because of the magnetic field, the parallel and transverse polarizabilities are not equal.

Combining Eqs. (12) and (16) with the relation $\mathbf{d}=\hat{\alpha}\cdot\boldsymbol{\mathcal{E}}$ yields the expressions

$$d_z=\alpha_z E_z$$

$$\left(1-\frac{\alpha_\perp B^2}{MC^2}\right)\mathbf{d}_\perp=\alpha_\perp\left[\mathbf{E}_\perp+\frac{1}{c}\frac{d\langle\mathbf{R}_{cm}\rangle}{dt}\times B\right]. \tag{17}$$

Substituting these expressions into Eq. (13) yields the equation of motion

$$M\left(1-\frac{\alpha_\perp B^2}{MC^2}\right)\frac{dV_z}{dt}\hat{z}+M\frac{d\mathbf{V}_\perp}{dt}=\frac{1}{2}\boldsymbol{\nabla}\left[\left(1-\frac{\alpha_\perp B^2}{MC^2}\right)\alpha_z E_z^2+\alpha_\perp E_\perp^2\right]+\alpha_\perp\frac{\mathbf{V}_\perp\times\mathbf{B}}{c}\cdot\boldsymbol{\nabla}\mathbf{E}+\alpha_\perp\frac{\mathbf{V}}{c}\cdot\boldsymbol{\nabla}(\mathbf{E}\times\mathbf{B}), \tag{18}$$

where $\mathbf{V}\equiv d\langle\mathbf{R}_{cm}\rangle/dt$, $\mathbf{E}$ is evaluated at $\langle\mathbf{R}_{cm}\rangle$, α_z and $\alpha_\perp$ have been treated as constants, and use has been made of $\boldsymbol{\nabla}\times\mathbf{E}=0$. Taking the dot product of Eq. (18) with respect to $\mathbf{V}$ and integrating over time yields an equation for conservation of energy

$$\left(1-\frac{\alpha_\perp B^2}{MC^2}\right)\frac{MV_z^2}{2}+\frac{MV_\perp^2}{2}-\frac{\alpha_\perp E_\perp^2}{2}-\alpha_z\left(1-\frac{\alpha_\perp B^2}{MC^2}\right)\frac{E_z^2}{2}=\text{const}, \tag{19}$$

where again use has been made of $\boldsymbol{\nabla}\times\mathbf{E}=0$.

It is convenient to introduce cylindrical coordinates for the center of mass, $\mathbf{R}_{cm}=(R,\Theta,Z)$. Typically, the electric potential has no dependence on the angle Θ, and the azimuthal electric field vanishes. In this case, Eq. (18) yields an equation for conservation of canonical angular momentum

$$\left(1-\frac{\alpha_\perp B^2}{MC^2}\right)^{-1}\left[MV_\theta R+\frac{\alpha_\perp B}{c}RE_R(R,Z)\right]=\text{const}. \tag{20}$$

Formal expressions for α_z and $\alpha_\perp$ can be obtained in terms of the energy levels for the relative motion, $\overline{H}_{n_1,n_2,n_3}(\mathcal{E}_z,\mathcal{E}_\perp)$. In the adiabatic approximation considered here, the quantum numbers for the state [i.e., (n_1,n_2,n_3)] remain fixed but the energy levels evolve as a function of the slowly varying $\mathcal{E}_z$ and $\mathcal{E}_\perp$. From the relations $-ez=\partial H/\partial\mathcal{E}_z$ and $\langle\Psi|\partial H/\partial\mathcal{E}_z|\Psi\rangle=\partial/\partial\mathcal{E}_z\langle\Psi|H|\Psi\rangle$, one finds that

$$d_z\equiv\langle ez\rangle=-\frac{\partial}{\partial\mathcal{E}_z}\overline{H}_{n_1,n_2,n_3}(\mathcal{E}_z,\mathcal{E}_\perp). \tag{21}$$

Likewise, one finds that

$$\mathbf{d}_\perp\equiv\langle e\mathbf{r}_\perp\rangle=-\frac{\partial}{\partial\boldsymbol{\mathcal{E}}_\perp}\overline{H}_{n_1,n_2,n_3}(\mathcal{E}_z,\mathcal{E}_\perp). \tag{22}$$

The linear polarizabilities are then given by

$$\alpha_z=-\left.\frac{\partial^2\overline{H}}{\partial^2\mathcal{E}_z^2}\right|_{\mathcal{E}_z,\mathcal{E}_\perp=0}\qquad\alpha_\perp=-\left.\frac{\partial^2\overline{H}}{\partial^2\mathcal{E}_\perp^2}\right|_{\mathcal{E}_z,\mathcal{E}_\perp=0}. \tag{23}$$

III. POLARIZABILITY FOR GUIDING CENTER DRIFT ATOMS

In this section, we evaluate the polarizability for the weakly bound and strongly magnetized atoms produced in the antihydrogen experiments. In recent literature, these atoms are referred to as guiding center drift atoms.[4–6] The cyclotron frequency for the positron is much larger than the other frequencies that characterize the dynamics, and the cyclotron radius much smaller than the positron-antiproton separation. Under these circumstances, the rapid and highly localized cyclotron motion can be averaged out and the pos-

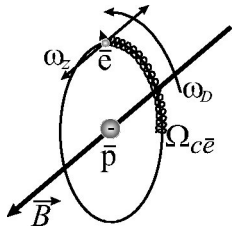

FIG. 1. Drawing of a guiding center drift atom. In order of descending frequency, the positron executes cyclotron motion, oscillates back and forth along a field line in the Coulomb well of the antiproton, and $\mathbf{E}\times\mathbf{B}$ drifts around the antiproton.

itron dynamics treated by guiding center drift theory. A quasiclassical treatment of the atoms is possible, since the binding energy is much smaller (four orders of magnitude smaller) than the Rydberg energy.

Figure 1 illustrates the internal dynamics (relative motion) of a guiding center drift atom for the special case where the effective electric field vanishes (i.e., $\boldsymbol{\mathcal{E}}\rightarrow 0$). The positron executes very rapid cyclotron motion with a small cyclotron radius. More slowly, the positron oscillates back and forth along the magnetic field in the Coulomb well of the antiproton. More slowly still, the positron and antiproton move in circular cross magnetic field orbits around a common point. The positron cross field motion is well described as the $\mathbf{E}\times\mathbf{B}$ drift velocity in the electric field of the antiproton, but full dynamics must be retained to describe the cross field motion of the antiproton. In Fig. 1, $\mathbf{r}=\mathbf{r}_1-\mathbf{r}_2$ is the relative position so the motion is shown from the perspective of the antiproton.

The relative motion is described by Hamiltonian (14) with the effective electric field set equal to zero (i.e., $\boldsymbol{\mathcal{E}}=0$). We will see that the first two terms describe the rapid cyclotron motion, the next two the field aligned oscillations, and the third and fourth the cross field motion. The cyclotron frequency is $\sqrt{1-4\mu/M}\ eB/\mu c\simeq eB/m_e c\equiv\Omega_{\mathrm{ce}}$. For the case where the amplitude of the field aligned oscillations is not too large (i.e., $z_{\max}\lesssim r_\perp=\sqrt{x^2+y^2}$), the frequency of these oscillations is approximately $\omega_z=\sqrt{e^2/m_e r_\perp^3}$. This estimate has used the Taylor expansion $e^2/\sqrt{z^2+r_\perp^2}\approx e^2/r_\perp - e^2z^2/2r_\perp^3$. For this same case, we will see that the frequency of the cross field motion is approximately $\omega_D+\Omega_{\mathrm{CM}}$, where $\omega_D\equiv ce/Br_\perp^3$ is the $\mathbf{E}\times\mathbf{B}$ drift frequency of a positron in the Coulomb field of a stationary antiproton. We will be interested in cases where $\omega_D\gtrsim\Omega_{\mathrm{CM}}$, so we simply use ω_D as the estimate of the frequency for cross field motion.

Since the positron cyclotron frequency, $\Omega_{\mathrm{ce}}=eB/m_e c$, is related to $\omega_z=\sqrt{e^2/m_e r_\perp^3}$ and $\omega_D=ce/Br_\perp^3$ through the equation $\Omega_{\mathrm{ce}}=\omega_z^2/\omega_D$, the requirement that Ω_{ce} be larger than the other two frequencies imposes the ordering

$$\Omega_{\mathrm{ce}}\gg\omega_z\gg\omega_D. \tag{24}$$

The ordering is realized for sufficiently weak binding, that is, for $r\gg(m_e c^2/B^2)^{1/3}$. This inequality is required for validity of the analysis.

Note that the inequality implies not only that the positron cyclotron frequency is large, but also that the positron cyclotron radius is small. We have in mind cases where the positron kinetic energy is smaller than or of order of the electrostatic binding energy (i.e., $m_e v_e^2/2\lesssim e^2/r$). The inequality $r\gg(m_e c^2/B^2)^{1/3}$ then implies that $r_{\mathrm{ce}}\equiv v_e/\Omega_{\mathrm{ce}}\ll r$.

For r comparable to $(m_e c^2/B^2)^{1/3}$ our guiding center analysis fails. All three frequencies in inequality (24) are comparable, and the positron motion is chaotic.[5,9,10] For $r\ll(m_e c^2/B^2)^{1/3}$, the cyclotron frequency is small compared to the Kepler frequency, and the positron motion is again integrable. In this case, one can think of the weakly bound pair as a high-n Rydberg atom with a Zeeman perturbation.[11] For cases where $r<(m_e c^2/B^2)^{1/3}$, equation of motion (18) remains valid, but the polarizability derived here does not apply.

As mentioned, the ATRAP collaboration measured binding energies of order meV, which corresponds to $\bar{e}-\bar{p}$ separation of order 10^{-4} cm.[3] The magnetic field strength is 5 T, so the critical radius is $(m_e c^2/B^2)^{1/3}=7\times10^{-6}$ cm. Thus, the separation is much larger than $(m_e c^2/B^2)^{1/3}$, and the weakly bound pairs are guiding center atoms. The cyclotron frequency for the positron is about 100 times larger than the $\mathbf{E}\times\mathbf{B}$ drift frequency ω_D, and the cyclotron radius is about 100 times smaller than the separation.

The simple symmetry of the orbit shown in Fig. 1 is a consequence of the choice $\boldsymbol{\mathcal{E}}=0$. For nonzero $\boldsymbol{\mathcal{E}}$, the last term in Hamiltonian (14) modifies the motion, but for sufficiently small $\boldsymbol{\mathcal{E}}$ the modifications can be treated as a perturbation. The term $e\mathcal{E}_z z$ shifts the field aligned oscillations, destroying symmetry of the orbit in $\pm z$. Likewise, the term $e\boldsymbol{\mathcal{E}}_\perp\cdot\mathbf{r}_\perp$ destroys the circular symmetry of the cross field orbit. Of course, these distortions give rise to the polarization of interest.

Because the atom moves, the effective field $\boldsymbol{\mathcal{E}}=\boldsymbol{\mathcal{E}}[\langle\mathbf{R}_{\mathrm{cm}}\rangle(t)]$ varies in time. As mentioned earlier, we assume that the time scale for this motion (i.e., $\tau\sim\ell/V_{\mathrm{cm}}$) is long compared to the time scale for the internal dynamics. Thus, frequency ordering (24) is extended to be

$$\Omega_{\mathrm{ce}}\gg\omega_z\gg\omega_D\gg 1/\tau. \tag{25}$$

The frequency ordering then implies that the internal dynamics for the atom is integrable. Because the positron cyclotron frequency is much larger than the other frequencies, the cyclotron action is a good adiabatic invariant. Use of guiding center drift dynamics automatically takes this invariant into account and removes the rapid cyclotron motion from the problem. Because the frequency of field aligned oscillations is larger than the remaining frequencies, the action for the field aligned oscillations is a good adiabatic invariant. Introducing this action and averaging over the field aligned oscillations then leaves the cross field drift motion as the largest frequency motion. Thus, the drift action is a good adiabatic invariant. The values of these three actions determine the internal state of the atom. In Ref. 5, Bohr-Sommerfeld quantization rules are used to associate a quantum number with each action. To the extent that $1/\tau$ is small compared to the frequencies for the internal dynamics [i.e., ordering (25)], the adiabatic approximation implies that the actions (or quantum numbers) remain constant as the atom moves through the external field. In the language of atomic physics, we make a triple Born-Oppenheimer approximation.

Returning to Hamiltonian (14) with frequency ordering (25) in mind, we first treat the cyclotron motion. The first two terms in Eq. (14) comprise the cyclotron Hamiltonian

$$H_c = \frac{p_x^2}{2\mu} + \frac{\left(p_y - \sqrt{1-\frac{4\mu}{M}}\frac{eBx}{c}\right)^2}{2\mu}, \tag{26}$$

where p_y may be treated as a constant on the cyclotron time scale. The Hamiltonian describes oscillations in x at the frequency $eB/\mu c\sqrt{1-4\mu/M} \simeq \Omega_{ce}$ and centered about the guiding center position $x_g = p_y(c/eB)(1-4\mu/M)^{1/2} \simeq cp_y/eB$. By introducing the cyclotron action,

$$I_c = \frac{1}{2\pi}\oint dx p_x(\overline{H}_c, x), \tag{27}$$

one finds $\overline{H}_c = I_c\Omega_{ce}$. Here, $\overline{H}_c$ has the same value as H_c but a different functional form. Making this replacement for the first two terms in Hamiltonian (14) and replacing x by $x_g = cp_y/eB$ in the remainder of the Hamiltonian yields the guiding center drift Hamiltonian[5]

$$H = I_c\Omega_{ce} + \frac{p_z^2}{2\mu} - \frac{e^2}{\sqrt{r_\perp^2+z^2}} - e\mathcal{E}_z z + \frac{M\Omega_{CM}^2}{2}r_\perp^2 - e\boldsymbol{\mathcal{E}}_\perp\cdot\mathbf{r}_\perp, \tag{28}$$

where $\mathbf{r}_\perp = (cp_y/eB, y)$. In drift dynamics, y and $p_y = eBx/c$ are canonically conjugate coordinate and momentum.[12] The field aligned oscillations are governed by the second, third, and fourth terms in Hamiltonian (28). We write the sum of these terms as the Hamiltonian

$$H_z = \frac{p_z^2}{2\mu} - \frac{e^2}{\sqrt{r_\perp^2+z^2}} - e\mathcal{E}_z z, \tag{29}$$

where $r_\perp$ can be treated as constant on the time scale of the field aligned oscillations. The action for the field aligned oscillations is given by

$$I_z = \frac{1}{2\pi}\oint dz\sqrt{2\mu}\sqrt{\overline{H}_z + e^2/(r_\perp^2+z^2)^{1/2} + e\mathcal{E}_z z}, \tag{30}$$

which can be inverted at least formally, to obtain $\overline{H}_z = \overline{H}_z(r_\perp^2, I_z, \mathcal{E}_z)$. Again, $\overline{H}_z$ has the same value as H_z but different functional form.

Substituting $\overline{H}_z(r_\perp^2, I_z, \mathcal{E}_z)$ into Eq. (28) yields a Hamiltonian for the cross field motion

$$H = I_{ce}\Omega_{ce} + \overline{H}_z(r_\perp^2, I_z, \mathcal{E}_z) + \frac{M\Omega_{CM}^2}{2}r_\perp^2 - e\boldsymbol{\mathcal{E}}_\perp\cdot\mathbf{r}_\perp. \tag{31}$$

For given values of H, I_{ce}, I_z, $\mathcal{E}_z$, and $\boldsymbol{\mathcal{E}}_\perp$ this equation determines the cross field orbit [i.e., $p_y(y)$, where $p_y = (eB/c)x$]. It is useful to introduce the action for the cross field motion (drift action)

$$I_D = \frac{1}{2\pi}\oint dy p_y[y, \overline{H} - \Omega_{ce}I_c, I_z, \mathcal{E}_z, \mathcal{E}_\perp], \tag{32}$$

which can be inverted formally to obtain $\overline{H} = \overline{H}(I_c, I_z, I_D, \mathcal{E}_z, \mathcal{E}_\perp)$. Following Ref. 5, the Bohr-Sommerfeld rules for quantization are used to set

$$\overline{H} = \overline{H}[I_c = \hbar n_c, I_z = \hbar n_z, I_D = \hbar n_D, \mathcal{E}_z, \mathcal{E}_\perp], \tag{33}$$

where the integers n_c, n_z, n_D remain fixed as $\boldsymbol{\mathcal{E}} = \boldsymbol{\mathcal{E}}[\langle\mathbf{R}_{cm}\rangle(t)]$ evolves slowly in time. In expression (23) for the polarizability, the energy levels are simply $\overline{H}_{n_1,n_2,n_3} = \overline{H}(\hbar n_c, \hbar n_z, \hbar n_D, \mathcal{E}_z, \mathcal{E}_\perp)$, where $(n_1, n_2, n_3) = (n_c, n_z, n_D)$.

For linear polarizability, $\alpha_z = -\partial^2\overline{H}/\partial\mathcal{E}_z^2|_{\mathcal{E}_z,\mathcal{E}_\perp=0}$ can be evaluated setting $\mathcal{E}_\perp = 0$ at the outset. In this case the cross field orbit is circular and the drift action is simply

$$I_D = \frac{1}{2\pi}\oint p_y dy = \frac{eB}{2c}r_\perp^2. \tag{34}$$

Substituting this expression for $r_\perp^2$ in Eq. (31) and setting $\boldsymbol{\mathcal{E}}_\perp = 0$ yields the energy levels $\overline{H} = \overline{H}(I_c, I_z, I_D, \mathcal{E}_z, \mathcal{E}_\perp = 0)$.

The partial derivative of this equation with respect to $\mathcal{E}_z$ yields the dipole moment

$$d_z = -\frac{\partial\overline{H}}{\partial\mathcal{E}_z} = -\frac{\partial\overline{H}_z}{\partial\mathcal{E}_z}. \tag{35}$$

By taking the derivative of Eq. (30) with respect to $\mathcal{E}_z$ holding I_z and $r_\perp^2 = [2c/(eB)]I_D$ constant, we obtain the equation

$$0 = \frac{1}{2\pi}\oint\frac{dz}{\dot{z}(z)}\left[\frac{\partial\overline{H}_z}{\partial\mathcal{E}_z} + ez\right], \tag{36}$$

where

$$\dot{z} = \pm\sqrt{\frac{2}{\mu}}\sqrt{\overline{H}_z + e^2/(r_\perp^2+z^2)^{1/2} + e\mathcal{E}_z z}. \tag{37}$$

In Eq. (36) $\overline{H}_z(I_z, r_\perp^2, \mathcal{E}_z)$ is independent of z, so we obtain the result

$$d_z = -\frac{\partial H_z}{\partial\mathcal{E}_z} = \frac{\oint\frac{dz}{\dot{z}(z)}ez}{\oint\frac{dz}{\dot{z}(z)}}. \tag{38}$$

Thus, the dipole moment is expressed as the time average of ez over the semiclassical orbit. In Sec. II [see Eq. (13)], the dipole moment was written as the expectation value $\langle e\mathbf{r}\rangle$. Here, we see that the expectation value goes over to a time average in the semiclassical limit.

To determine α_z, we evaluate time average (38) numerically with $\dot{z} = \dot{z}(z, H_z, r_\perp, \mathcal{E}_z)$ given by Eq. (37). For sufficiently small $\mathcal{E}_z$, d_z is linear in $\mathcal{E}_z$ and $\alpha_z = d_z/\mathcal{E}_z$ is independent of $\mathcal{E}_z$. Removal of dependence on $\mathcal{E}_z$ allows the result for the linear α_z to be presented in a completely scaled form. Figure 2 shows the scaled polarizability $\alpha_z|H_z|^3/e^6$ versus the scaled radius $|H_z|r_\perp/e^2$.

It is instructive to note alternate forms for these scaled variables. In Fig. 3 of Ref. 5 the scaled radius $|H_z|r_\perp/e^2$ is given as a function of the ratio $I_z/\sqrt{r_\perp}$, where I_z is the action for the field aligned oscillations. Large I_z corresponds to small $|H_z|r_\perp/e^2$, and $I_z = 0$ corresponds to $|H_z|r_\perp/e^2 = 1$. Also, in the small field limit the magnitude of Hamiltonian (29) can be written as $|H_z| = e^2/\sqrt{r_\perp^2 + z_{max}^2}$, where z_{max} is the am-

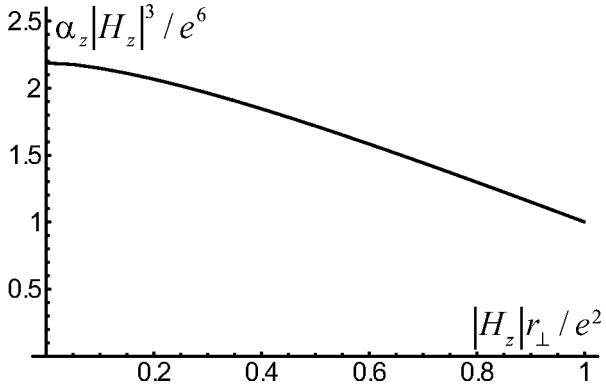

FIG. 2. The scaled polarizability $\alpha_z|H_z|^3/e^6$ vs the scaled radius $|H_z|r_\perp/e^2$.

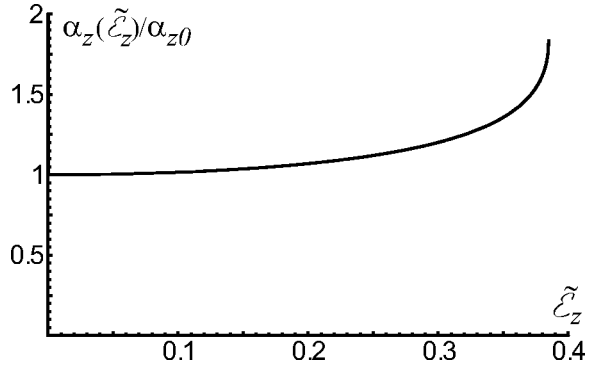

FIG. 4. Nonlinear scaled polarizability α_z for the case of $I_z=0$. In this plot $\alpha_{z0}=r_\perp^3$ and $\tilde{\mathcal{E}}_z=\mathcal{E}_z r_\perp^2/e$.

plitude of the field aligned oscillations. Thus, the scaled polarizability can be written as $\alpha_z|H_z|^3/e^6=\alpha_z/(r_\perp^2+z_{\max}^2)^{3/2}$ and the scaled radius as $|H_z|r_\perp/e^2=r_\perp/\sqrt{r_\perp^2+z_{\max}^2}$.

Referring again to Fig. 2, we note that for $|H_z|r_\perp/e^2=r_\perp/\sqrt{r_\perp^2+z_{\max}^2}$ near unity (i.e., small $z_{\max}/r_\perp$), α_z takes the value $r_\perp^3$. For $|H_z|r_\perp/e^2$ near zero, α_z is given by $(35/16)z_{\max}^3$. Analytic solutions are possible at both end points. The small I_z value of the polarization (i.e., $\alpha_z=r_\perp^3$) has been noted earlier.[6]

To gain some idea of the range of $\mathcal{E}_z$ for which the linear theory is valid, we first review previous results on field ionization. Clearly, the critical field for ionization is an upper bound on the range of validity. Figure 3, which is taken from Ref. 5, shows the scaled critical field $\mathcal{E}_z/(H_z^2/e^3)$ versus the scaled radius $|H_z|r_\perp/e^2$. Here, the atom starts in a low field region and moves up a field gradient until field ionization occurs. As the atom moves, the action I_z is conserved until just before ionization. In contrast, the value of $H_z=H_z(\mathcal{E}_z,r_\perp,I_z)$ is not conserved. In Fig. 3, the value of $|H_z|$ that enters the scaled variables is the value in the low field region. Thus, the scaled radius in Fig. 3 is the same as that in Fig. 2. Also, note that the scaled field variable can be rewritten as $\mathcal{E}_z/(H_z^2/e^3)=\mathcal{E}_z(r_\perp^2+z_{\max}^2)/e$, where $z_{\max}$ is the amplitude of the z oscillations in the low field region. At the end point $|H_z|r_\perp/e^2=1$ the critical field is $\mathcal{E}_z=[2/(3\sqrt{3})]e/r_\perp^2\simeq 0.39e/r_\perp^2$, and at the end point $|H_z|r_\perp/e^2=0$ the critical field $\mathcal{E}_z=0.32e/z_{\max}^2$.

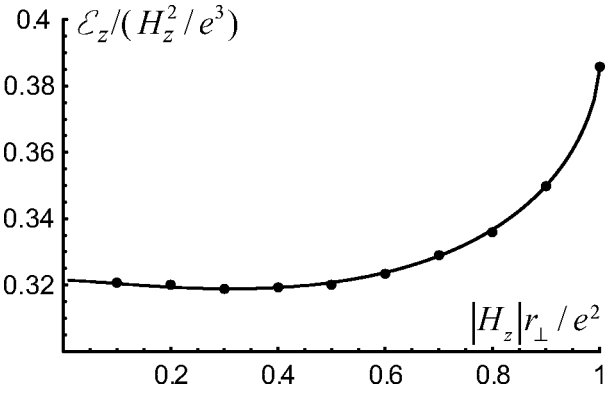

FIG. 3. Ionization by an electric field parallel to the magnetic field. $\mathcal{E}_z$ is the critical field for ionization, H_z is the initial binding energy before the atom enters the electric field, and $r_\perp$ is the radius of the nearly circular initial drift orbit. The solid curve results from a theory based on constancy of I_z, and the points are numerical solutions of coupled positron-antiproton equations of motion.

The end point $|H_z|r_\perp/e^2=1$ corresponds to $I_z=0$. For this limit, a nonlinear expression for α_z can be obtained analytically. The second two terms in Hamiltonian (29) provide a potential well with the bottom shifted toward positive z (for $\mathcal{E}_z>0$). For small I_z, the positron executes small amplitude oscillations near the bottom of the well. The oscillations are symmetric about the bottom since the well is approximately quadratic near the bottom. Thus, the time-average $\langle z\rangle$ is simply the z value of the shifted bottom.

Setting $\partial H_z/\partial z=0$ to determine the shifted bottom yields the result

$$\alpha_z=\frac{d_z}{\mathcal{E}_z}=r_\perp^3 g(\tilde{\mathcal{E}}_z), \tag{39}$$

where the scaled field is $\tilde{\mathcal{E}}_z=\mathcal{E}_z/(e/r_\perp^2)$ and

$$g(\tilde{\mathcal{E}}_z)=\frac{1}{\tilde{\mathcal{E}}_z}\left(\frac{2}{\sqrt{3}}\frac{1}{\tilde{\mathcal{E}}_z}\cos\left\{\frac{1}{3}\left[\pi+\arccos\left(\frac{3\sqrt{3}}{2}\tilde{\mathcal{E}}_z\right)\right]\right\}-1\right)^{1/2}$$
$$\equiv\frac{\alpha_z(\tilde{\mathcal{E}}_z)}{\alpha_{z0}}. \tag{40}$$

Here $\alpha_{z0}=r_\perp^3$, the value of α_z for $I_z=0$ and $\mathcal{E}_z=0$. Function (40) is plotted in Fig. 4. For small values of the scaled field, $g(\tilde{\mathcal{E}}_z)$ is near unity so that $\alpha_z\simeq r_\perp^3$ in accord with the linear value in Fig. 2. $g(\tilde{\mathcal{E}}_z)$ rises to its maximum value of $3\sqrt{3}/(2\sqrt{2})$ at $\tilde{\mathcal{E}}_z=2/(3\sqrt{3})$. At this upper limit, the well ceases to exist and the atom undergoes field ionization. Note that the value $\tilde{\mathcal{E}}_z=2/(3\sqrt{3})$ is the critical field predicted in Fig. 3 for end point $|H_z|r_\perp/e^2=1$.

To evaluate $\mathbf{d}_\perp$ and $\alpha_\perp$, we first make a canonical transformation from the cross field variables $[y,p_y=(eB/c)x]$ to $[\theta,p_\theta=eBr_\perp^2/(2c)]$, where $\theta=0$ is in the direction $\boldsymbol{\mathcal{E}}_\perp$. Hamiltonian (31) then takes the form

$$H = I_c\Omega_{ce} + \overline{H}_z\left[\frac{2c}{eB}p_\theta, I_z, \mathcal{E}_z = 0\right] + \frac{M\Omega_{CM}^2}{2}\left(\frac{2c}{eB}p_\theta\right) - e\mathcal{E}_\perp\sqrt{(2c/eB)p_\theta}\cos\theta, \tag{41}$$

where $\mathcal{E}_z$ has been set equal to zero. For the circular orbits considered above, p_θ itself is the drift action, but for the noncircular orbits considered here the drift action is given by

$$I_D = \frac{1}{2\pi}\oint p_\theta[\overline{H} - \Omega_{ce}I_c, I_z, \mathcal{E}_z = 0, \mathcal{E}_\perp, \theta]d\theta. \tag{42}$$

Taking the derivative with respect to $\mathcal{E}_\perp$, holding the actions constant, yields the relation

$$0 = \frac{1}{2\pi}\oint\left[\frac{\partial p_\theta}{\partial H}\frac{\partial \overline{H}}{\partial E_\perp} + \frac{\partial p_\theta}{\partial \mathcal{E}_\perp}\right]d\theta. \tag{43}$$

Using $\dot{\theta} = \partial H/\partial p_\theta$ and $\partial p_\theta/\partial\mathcal{E}_\perp = -\partial H/\partial\mathcal{E}_\perp/(\partial H/\partial p_\theta) = er_\perp\cos\theta/\dot{\theta}$ we again find that the dipole moment is given by a time average over the semiclassical orbit

$$d_\perp = -\frac{\partial H}{\partial \mathcal{E}_\perp} = \frac{\oint \frac{d\theta}{\dot{\theta}(\theta)} r_\perp(\theta)\cos\theta}{\oint \frac{d\theta}{\dot{\theta}(\theta)}}. \tag{44}$$

To determine $\alpha_\perp$ we use time average (44) together with Hamiltonian (41). For small $\mathcal{E}_\perp$ and small I_z, a simple perturbation treatment yields an analytic expression for the linear $\alpha_\perp$. For small I_z, the term $\overline{H}_z(r_\perp, I_z)$ in Eq. (41) can be approximated as[5]

$$\overline{H}_z(r_\perp, I_z) \simeq -\frac{e^2}{r_\perp} + I_z\omega_z(r_\perp), \tag{45}$$

where $\omega_z(r_\perp) = \sqrt{e^2/(\mu r_\perp^3)}$ is the frequency of small amplitude field aligned oscillations and $r_\perp$ is shorthand for $\sqrt{2cp_\theta/(eB)}$. In the following, we use these two expressions for $r_\perp$ interchangebly, always being cautious to note that $[\theta, p_\theta = eBr_\perp^2/(2c)]$ are canonically conjugate variables.

In the small field limit, we set $r_\perp(\theta) = r_\perp + \delta r_\perp(\theta)$ and solve for $\delta r_\perp(\theta)$ to first order in $\mathcal{E}_\perp$ using Hamiltonian (41) and approximation (45). The result is

$$\delta r_\perp(\theta) = \frac{(\mathcal{E}_\perp/e)r_\perp^3\cos\theta}{1 + B^2r_\perp^3/(Mc^2) - 3I_z/(2\sqrt{r_\perp\mu e^2})}. \tag{46}$$

Substituting $r_\perp(\theta) = r_\perp + \delta r_\perp(\theta)$ into each term of time average (44), including both the term $r_\perp(\theta)\cos\theta$ and the term $\dot{\theta}[\theta, r_\perp(\theta)] = \partial H/\partial p_\theta$, and then linearizing in $\mathcal{E}_\perp$ yields the polarizability

$$\alpha_\perp = \frac{d_\perp}{\mathcal{E}_\perp} = \frac{5}{2}r_\perp^3\frac{1 + \frac{2}{5}\frac{B^2r_\perp^3}{Mc^2} - \frac{33}{20}\frac{I_z}{\sqrt{\mu r_\perp e^2}}}{\left(1 + \frac{B^2r_\perp^3}{Mc^2} - \frac{3}{2}\frac{I_z}{\sqrt{\mu r_\perp e^2}}\right)^2}. \tag{47}$$

In this expression, the quantity $I_z/\sqrt{\mu r_\perp e^2}$ can be replaced by $z_{max}^2/(2r_\perp^2)$, since I_z is small.

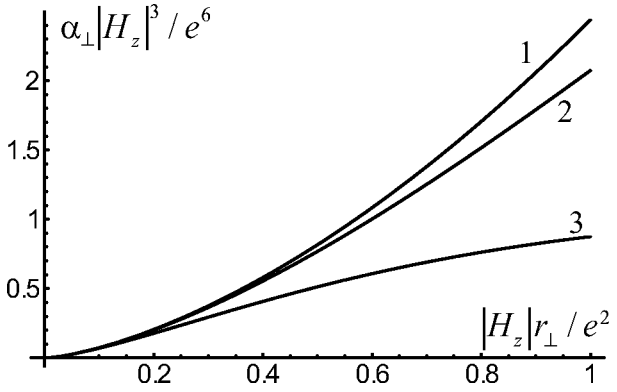

FIG. 5. Scaled polarizability $\alpha_\perp|H_z|^3/e^6$ vs the scaled radius $|H_z|r_\perp/e^2$. The three curves correspond to the β values: (1) $\beta = 0.015\,625$, (2) $\beta = 0.125$, (3) $\beta = 1$.

This small field (linear) calculation of $\alpha_\perp$ can be carried out numerically for arbitrary I_z, that is, without invoking approximation (45). Figure 5 shows plots of the scaled polarizability $\alpha_\perp|H_z|^3/e^6$ versus the scaled radius $|H_z|r_\perp/e^2$ for several values of the parameter $\beta = e^6B^2/(|H_z|^3Mc^2)$. These curves are analogous to the curve in Fig. 3 for $\alpha_z|H_z|^3/e^6$ versus $|H_z|r_\perp/e^2$. Here, more than one curve is required to present the results, since $\alpha_\perp|H_z|^3/e^6$ depends on two parameters: $|H_z|r_\perp/e^2$ and $\beta = e^6B^2/(|H_z|^3Mc^2)$. One can easily check that approximate expression (47) can be scaled with these variables. In this regard note that $I_z/\sqrt{\mu r_\perp e^2} = 1 - |H_z|r_\perp/e^2$ for small I_z.

Figure 6 shows the scaled critical field for ionization $\mathcal{E}_\perp/(|H_z|^3/e^3)$ versus the scaled radius $|H_z|r_\perp/e^2$ for same three values of parameter β as in Fig. 5. The critical field is an upper limit on the range of validity for the small field (linear) results displayed in Fig. 5. Curves in Fig. 6 are displayed for values of $|H_z|r_\perp/e^2$ such that inequality (24) holds. If the scaled radius $|H_z|r_\perp/e^2$ becomes of order of $[\mu/(M\beta)]^{1/3}$ [or equivalently, $r_\perp$ becomes of order of $(\mu c^2/B^2)^{1/3}$], the frequencies in Eq. (24) become equal, and the guiding center drift approximation fails.

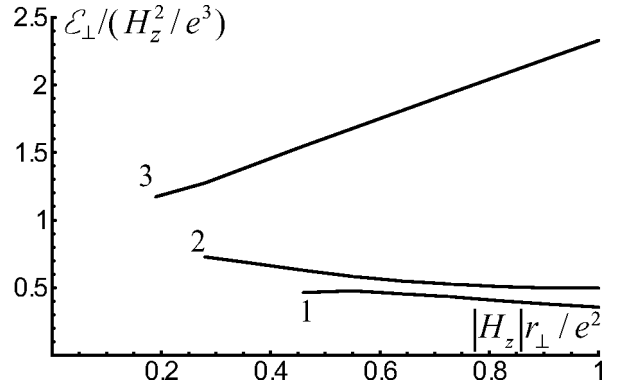

FIG. 6. Ionization by an electric field perpendicular to the magnetic field. $\mathcal{E}_\perp$ is the critical field for ionization, H_z is the initial binding energy before the atom enters the electric field, and $r_\perp$ is the radius of the nearly circular initial drift orbit. The three curves correspond to the β values: (1) $\beta = 0.015\,625$, (2) $\beta = 0.125$, (3) $\beta = 1$.

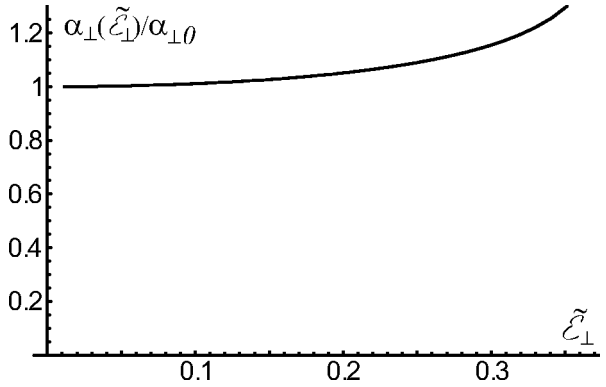

FIG. 7. Scaled polarizability $\alpha_\perp$ for the case $I_z=0$ and $\beta=0.0383$. In this plot $\alpha_{\perp 0}=(5/2)r_\perp^3[1+(2/5)\beta]/[1+\beta]^2$ and $\tilde{\mathcal{E}}_\perp=\mathcal{E}_\perp r_\perp^2/e$.

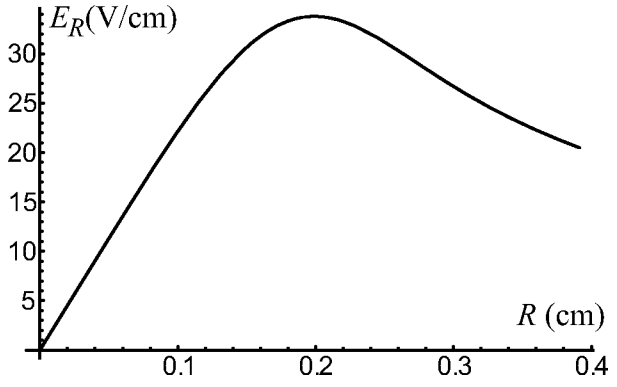

FIG. 8. Radial profile of the space charge electric field.

As the critical field is approached, the polarization becomes nonlinear. Figure 7 shows a plot of $\alpha_\perp/\alpha_{\perp 0}$ versus the scaled electric field $\tilde{\mathcal{E}}_\perp=\mathcal{E}_\perp/(|H_z|^2/e^3)=\mathcal{E}_\perp r_\perp^2/e$ for the case $I_z=0$. For this plot we chose a particular value of $\beta=0.0383$ that will be used in the next section. As in Fig. 4, $\alpha_\perp(\tilde{\mathcal{E}}_\perp)$ is scaled by the linear polarizability $\alpha_{\perp 0}$. Using Eq. (47) to express $\alpha_{\perp 0}$ in terms of $r_\perp$ and β yields the relation

$$\frac{\alpha_\perp(\tilde{\mathcal{E}}_\perp)}{\alpha_{\perp 0}}=\alpha_\perp(\tilde{\mathcal{E}}_\perp)\frac{2}{5r_\perp^3}\frac{(1+\beta)^2}{1+(2/5)\beta}. \tag{48}$$

If the electric field is small ($\mathcal{E}r_\perp^2/e<0.15$), the polarizability is nearly constant indicating a linear relation between the polarization and electric field. However for larger field, $\alpha_\perp$ increases with $\mathcal{E}_\perp$ as field ionization approached.

IV. MOTION OF THE GUIDING CENTER DRIFT ATOMS IN PENNING TRAP FIELDS

As a first application of approximate equation of motion (18), we consider the radial trapping of weakly bound atoms in the large space charge field near the edge of a long cylindrical positron column. Let (R,Θ,Z) be cylindrical coordinates for the atom center of mass. The fields must be expressed in these coordinates for use in Eq. (18). We choose a plasma density $n_0=2.5\times10^8$ cm^{-3} and plasma radius $R_p=0.2$ cm in accord with ATHENA parameters,[1] and for convenience take the (unknown) density profile to be simply $n(R)=n_0\exp[-(R/R_p)^4]$. For a long column, the corresponding space charge field is shown in Fig. 8. Also, in accord with ATHENA parameters we choose the magnetic field strength $B=3$T.

Figure 9 shows the orbit of a rather tightly bound guiding center atom ($r_\perp=2.4\times10^{-5}$ cm, $e^2/r_\perp=5.9$ meV, $I_z=0$) ejected in the azimuthal direction with rather small initial velocity $V_\Theta=2.4\times10^3$ cm/s. The figure actually shows two nearly identical curves. The solid curve is the solution of approximate equation (18) using polarizability $\alpha_\perp=3.6\times10^{-14}$ cm^3 calculated from Eq. (47). The dashed curve is the antiproton orbit from the solution of the coupled positron-antiproton equations of motion obtained from from Hamiltonian (7). This latter solution is difficult computationally since a million cycles of the internal dynamics must be followed. The rapid internal dynamics has been averaged out in Eq. (18). For this case of relatively tight binding and, consequently, shallow radial well, only atoms with small initial velocity are trapped. For example, the atom would have escaped, had it been given initial velocity 1.6×10^4 cm/s.

More shallowly bound atoms experience a deeper radial well and are confined for larger initial velocity. However, the polarizability can easily be in the nonlinear regime for these atoms. In the preceding section, we obtained the nonlinear polarizability $\alpha_\perp(\tilde{\mathcal{E}}_\perp)$ for an atom with parameters $r_\perp=4.0\times10^{-5}$ cm and $I_z=0$ (see Fig. 7). These parameters correspond to $|H_z|=e^2/r_\perp=3.6$ meV and $\beta=0.0383$ (for $B=3$ T). We assume that such an atom moves in the radial space charge field of Fig. 8. We anticipate that the trapped atom will sample a space charge field of $\mathcal{E}_\perp\simeq25$ V/cm, which corresponds to the scaled field $\tilde{\mathcal{E}}_\perp=0.27$. One can see from Fig. 7 that the polarizability is in the nonlinear regime for this field strength. We take the nonlinear value of the polarizability $\alpha_\perp(\tilde{\mathcal{E}}_\perp=0.27)\simeq1.18\alpha_{\perp 0}\simeq1.8\times10^{-13}$ cm^3, but

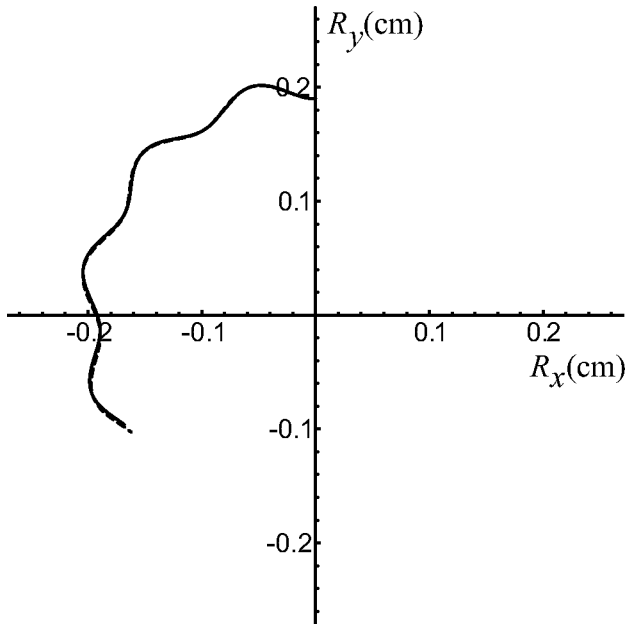

FIG. 9. Trapping of rather tightly bound atom ejected with small azimuthal velocity.

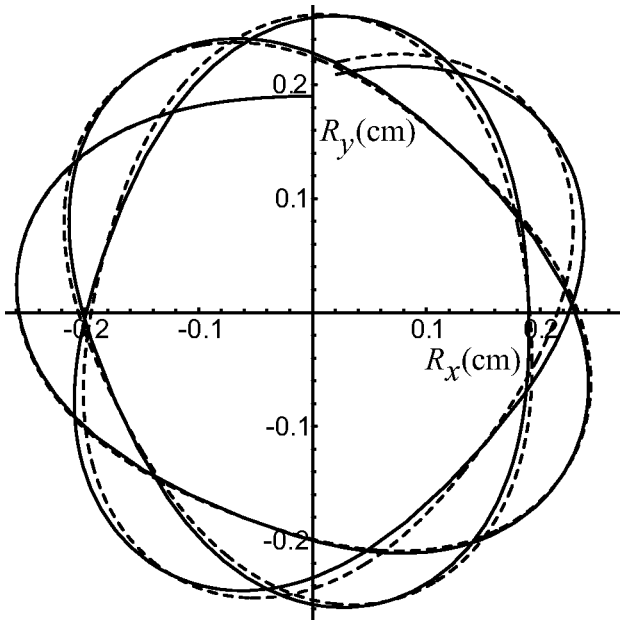

FIG. 10. Trapping of guiding center atom with higher initial velocity and shallower binding than in Fig. 9. Dashed curve is the ion orbit for a solution of the coupled positron-antiproton equations of motion. The continuous curve is the solution of approximate equations (18) with $\alpha = 1.18\alpha_{\perp 0}$.

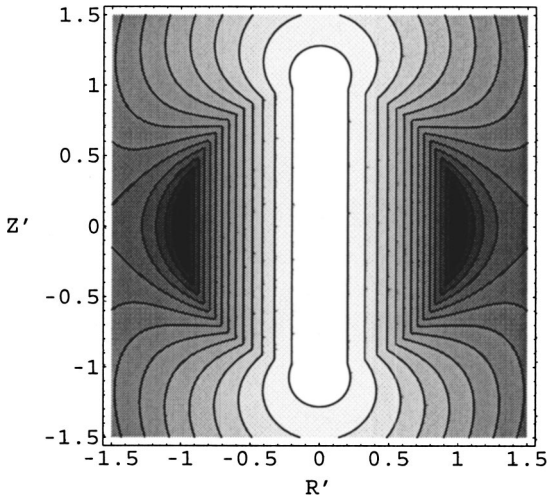

FIG. 11. Contour plot of scaled potential energy function $U(R',Z',2/5)$ for a spherical plasma equilibrium. Coordinates are scaled as $R'=R/r_p$ and $Z=Z/r_p$, where r_p is the radius of the spherical plasma. Deeper shading corresponds to lower values of U, so a toroidal potential well runs around the radial edge of the plasma.

treat the polarizability as constant. This anticipates the fact that the trapped atom samples a nearly constant field strength while moving in a nearly circular orbit.

Figure 10 shows the orbit of this guiding center drift atom launched with initial velocity ($V_\Theta = 2.7\times 10^4$ cm/s). This velocity corresponds to initial kinetic energy $MV_\Theta^2/2 = 0.38$ meV, as compared to a 1.3 meV temperature quoted for some ATHENA experiments. Again, the solid curve is the solution to Eq. (18), and the dashed curve is the solution to the coupled positron-antiproton equations of motion derived from Hamiltonian (7). In this case, the two curves are close, but can be distinguished, presumably because the nonlinear polarizability function $\alpha_\perp(E_\perp)$ was approximated by a single value. Both curves show that the atom is confined radially.

One expects that this mechanism produces radial trapping for some atoms in the ATHENA experiment. Near the edge of the positron column, where the space charge electric field is maximum (i.e., $E \simeq 30$ V/cm), the $\mathbf{E}\times\mathbf{B}$ drift velocity of an ion is $V_D \simeq 10^3$ m/sec. For the quoted temperature of $T \simeq 1.3$ meV, the thermal velocity is 500 m/sec. Thus, radial trapping can occur when atoms are born at a point in the ion orbit where the cyclotron velocity is directed opposite to the drift velocity. For example, if the cyclotron velocity were twice the mean thermal velocity, the atom would be born at rest in the laboratory frame.

We have been discussing radial trapping, but full three dimensional trapping is possible also. From Eq. (19) for conservation of energy, one can see that such trapping requires the potential energy function

$$V(R,Z) = -\frac{\alpha_\perp}{2}E_\perp^2(R_\perp,Z) - \frac{\alpha_Z}{2}\left(1-\frac{\alpha_\perp B^2}{MC^2}\right)E_Z^2(R,Z) \quad (49)$$

to be a three dimensional potential well. As a sample plasma equilibrium which produces such a well, we consider the simple case of a spherical positron plasma. In the Appendix, the fields $E_Z(R,Z)$ and $E_R(R,Z)$ are evaluated for a spherical positron plasma that is confined in a quadratic trap potential.[13] The plasma is assumed to be in a state of global thermal equilibrium, and the Debye length is assumed to be small compared to the radius of the plasma. Such plasmas have been studied extensively[13] and are regularly observed experimentally.[14] In the Appendix, the potential energy function is written in the form

$$V(R,Z) = -\frac{\alpha_\perp E^2}{2}U(R',Z',\gamma), \quad (50)$$

where E is the space charge field at the surface of the plasma sphere, and the dimensionless potential U depends on the scaled coordinates $R'=R/r_p$ and $Z'=Z/r_p$, where r_p is the radius of the sphere. The parameter β is the ratio $\gamma=\alpha_z(1-\alpha_\perp B^2/MC^2)/\alpha_\perp$. From Eqs. (39) and (47), one can see that the value $\gamma=2/5$ is correct for relatively deep binding and small I_z, that is, for $\alpha_\perp B^2/MC^2$, $I_z/\sqrt{\mu r_\perp e^2} \ll 1$. We use this value, but the existence of the potential well is not sensitive to this choice. An analytic expression for $U(R',Z',\beta)$ is given in Eq. (A5).

Figure 11 shows a contour plot of $U(R',Z',2/5)$. Deeper shading corresponds to lower values of U, so there is a toroidal potential well that runs around the radial edge of the plasma. The depth of the well is approximately $\Delta V \simeq (0.4)\alpha_\perp E^2$. Atoms that are born at the bottom of the well with center of mass kinetic energy less than $(0.4)\alpha_\perp E^2$ are trapped.

Using self-consistent numerical solutions, we have found three dimensional potential wells for other plasma equilibria (e.g., spheroidal plasmas and long columns). For example, the ATHENA plasma likely produces a three dimensional well with depth comparable to the radial well discussed above.

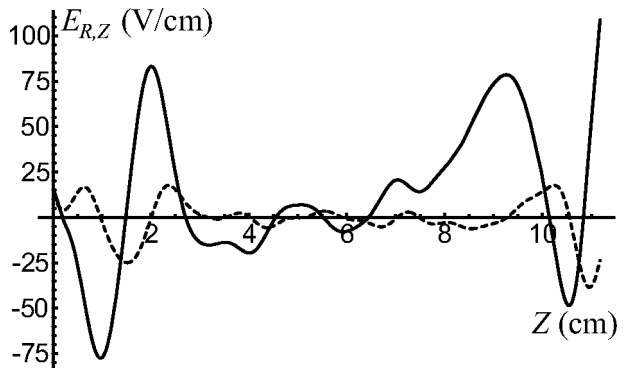

FIG. 12. Axial electric field $E_Z(R=0,Z)$ (solid line) and radial electric field $E_R(R=2\ \text{mm},Z)$ (dashed line) vs Z. These plots correspond to those reported in Fig. 2(c) of Ref. 3 for the ATRAP experiment.

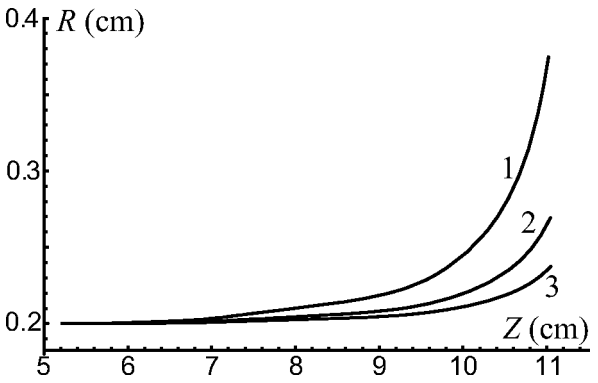

FIG. 13. Trajectories of an atom with binding energy $e^2/r_\perp=5.4$ meV and $I_z=0$ launched in the axial direction towards the ionization region with different initial velocities: (1) $V_Z=8.3\times10^4$ cm/s, (2) $V_Z=1.2\times10^5$ cm/s, (3) $V_Z=1.7\times10^5$ cm/s. The trajectories terminate at the point where E_z reaches the critical value for field ionization, $E_Z=80$ V/cm.

As another application of approximate equation of motion (18) we consider the curved trajectories followed by untrapped atoms in moving from the plasma to a field ionization region. Field ionization is the principle diagnostic used in the ATRAP experiments, so we use field strengths and geometry characteristic of ATRAP. The ATRAP collaboration previously estimated polarization forces parallel to the magnetic field, and correctly concluded that the forces produce a negligible change in parallel velocity for energetic atoms (i.e., $MV_Z^2/2\simeq200$ meV).[15] Here, we focus on slower atoms for which the forces are not negligible.

The space charge field is much smaller than the vacuum field used for field ionization, so to a good approximation the electrostatic potential satisfies Laplace's equation. Using cylindrical coordinates (R,Θ,Z) and noting that the potential is independent of Θ, we write the potential as a sum

$$\Phi(R,Z)=\sum_n\left[a_n\sin\left(\frac{2\pi nZ}{L}\right)+b_n\cos\left(\frac{2\pi nZ}{L}\right)\right]I_0\left(\frac{2\pi nR}{L}\right), \tag{51}$$

where I_0 is a Bessel function of imaginary argument, and the coefficients a_n and b_n are chosen so that the field $(E_R,E_Z)=(-\partial\Phi/\partial R,-\partial\Phi/\partial Z)$ provides a good approximation to the ATRAP field. In Fig. 2 of Ref. 3 the ATRAP field component $E_Z(R=0,Z)$ was reported for the range of Z values $L\simeq11.5$ cm. Retaining terms up to $n=15$ in the sum (51), we obtain the field components in Fig. 12 which compare well with those in Ref. 3.

Figure 13 shows the trajectories of atoms launched from a point within the positron plasma ($Z=5.5$ cm, $R=0.2$ cm) with three different center of mass velocities: (1) $V_Z=8.3\times10^4$ cm/s, (2) $V_Z=1.2\times10^5$ cm/s, (3) $V_Z=1.7\times10^5$ cm/s. The initial transverse velocity is zero for all three trajectories. The three initial velocities correspond to center of mass kinetic energy $MV_Z^2/2=3.6$ meV, 8.1 meV, and 14.4 meV. Initially the internal state of the atoms is characterized by $I_z=0$ and $r_\perp=2.6\times10^{-5}$ cm, which corresponds to binding energy $e^2/r_\perp=5.4$ meV. For this state, Eqs. (39) and (47) imply the linear polarizabilities $\alpha_z=1.8\times10^{-14}$ cm^3 and $\alpha_\perp=4.3\times10^{-14}$ cm^3. Shortly before field ionization, the polarizability becomes nonlinear and somewhat larger than the linear values used to calculate the trajectories. Thus, the trajectories slightly underestimate the deflection. Each trajectory ends when the critical field for ionization is reached [i.e., $E_Z=[2/(3\sqrt{3})](e/r_\perp^2)=80$ V/cm]. As one can see in Fig. 13, depending on initial axial velocity, radial deflection of the atom can be substantial due to polarization forces. The deflection is smaller for larger initial axial velocity because the atom spends less time in the region of high electric field.

Figure 14 shows the final radial position of the atom (i.e., at the moment of its field ionization) versus its initial radial position. As in Fig. 13, the atom was launched within the positron plasma at $Z=5.5$ cm but with different initial radial positions. The three curves in the figure correspond to the same three initial center of mass velocities as in Fig. 13. One can see in Fig. 14 that the radial deflection of the atom

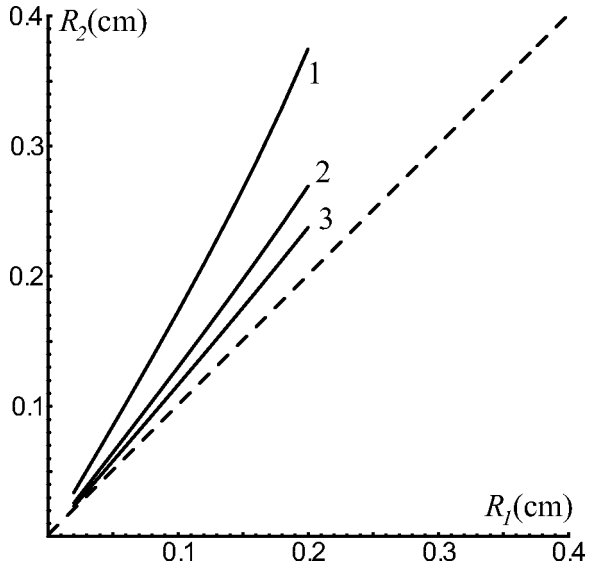

FIG. 14. Final radial position of the atom R_2 (at the moment of field ionization) vs its initial radial position R_1. Curves 1, 2, and 3 correspond to the same initial axial velocities as in Fig. 13. For reference, the dashed line shows $R_1=R_2$.

increases with increasing initial radial displacement. This is due to the fact that the electric fields grow radially in the field ionization region, so an atom launched at larger radius experiences larger electric field. Also, as in Fig. 13, one can see that radial deflection is reduced with increasing initial center of mass velocity.

A simple estimate of the deflection provides useful insight. The radial force on an atom is of order $F \simeq \partial/\partial R[\alpha E^2(R,Z)]$. For sufficiently small R, we can use the Taylor expansion

$$F \simeq R \left.\frac{\partial^2}{\partial R^2}[\alpha E^2(R,Z)]\right|_{R=0}, \tag{52}$$

where the constant term (zero order term) vanishes by symmetry. The scale length on which the field changes is R_W, the radius of the wall (electrode structure), so we set $\partial^2/\partial R^2[\alpha E^2(R,Z)] \simeq \alpha E^2/R_W^2$. Consider an atom that is born at radius $R=R_0$ with velocity $\mathbf{V}=V_Z\hat{z}$. The radial acceleration of the particle is $a=F/M=\alpha R_0 E^2/(MR_W^2)$. The field E^2 rises on a spatial scale $\Delta Z=R_W$ in the ionization region, so the approximate radial displacement is

$$\Delta R \simeq a\left(\frac{R_W}{V_Z}\right)^2 \simeq R_0\frac{\alpha E^2}{MV_Z^2}. \tag{53}$$

The polarizability is of order $\alpha \sim r_a^3$ and the field strength before ionization of order $E \sim e/r_a^2$, so the radial displacement is of order

$$\Delta R \simeq R_0\frac{e^2/r_a}{MV_Z^2}. \tag{54}$$

Thus, the deflection is substantial when the binding energy is comparable to the center of mass kinetic energy. The fact that the displacement is an increasing function of R_0 and a decreasing function of V_Z also is apparent.

ACKNOWLEDGMENTS

This work was supported by the National Science Foundation under Grant No. PHY9876999, and by the National Science Foundation and the Department of Energy under Grant No. PHY0354979.

The authors wish to thank Dr. Lars Jørgensen and Professor Gerald Gabrielse and Professor Fred Driscoll for helpful discussions.

APPENDIX: POTENTIAL ENERGY FUNCTION FOR A SPHERICAL POSITRON PLASMA

A commonly used trap potential is the quadratic potential,[13]

$$e\phi_T(R,Z) = \frac{m\omega_Z^2}{2}(Z^2 - R^2/2), \tag{A1}$$

where (R,Θ,Z) are cylindrical coordinates and ω_Z^2 is a constant that is proportional to the axial confinement voltage. The electrodes that produce this potential are assumed to be distant compared to the size of the plasma, so image potentials are negligible. There is also a uniform axial magnetic field, $\mathbf{B}=\hat{Z}B$.

We assume that the plasma has come to a state of global thermal equilibrium,[13] so the plasma rotates without shear at some frequency ω. In the rotating frame of the plasma, the effective trap potential is

$$e\phi_R(R,Z) = e\phi_T(R,Z) + m\omega(\Omega_{ce} - \omega)\frac{R^2}{2}, \tag{A2}$$

where $\Omega_{ce}=eB/m_e c$ is the positron cyclotron frequency. This effective potential has spherical symmetry, and the plasma consequently has spherical symmetry, if the frequencies are related as

$$\tfrac{3}{2}\omega_z^2 = \omega(\Omega_{ce} - \omega). \tag{A3}$$

We assume that the plasma Debye length is small compared to the plasma radius. In this case, the plasma density is nearly uniform out to some radius r_p and there drops to zero.[13] The density is specified by $\omega_p^2=2\omega(\Omega_{ce}-\omega)$, where ω_p^2 is the plasma frequency. From this relation and Eq. (A3), we easily obtain the plasma space charge potential $\phi_P(R,Z)$. The total potential in the laboratory frame is the sum $\phi(R,Z)=\phi_P(R,Z)+\phi_T(R,Z)$, and the fields required to evaluate potential energy function (51) are $E_R(R,Z) = -\partial\phi/\partial R$ and $E_Z(R,Z)=-\partial\phi/\partial Z$.

Substituting the fields into Eq. (51) yields the result

$$V(R,Z) = \frac{\alpha_\perp}{2}E^2 U(R',Z',\gamma), \tag{A4}$$

where $E=(m\omega_z^2 r_p/e)$ is the plasma space charge field at the surface of the plasma and

$$U(R',Z',\gamma) = -\begin{cases} \left(\frac{3}{2}R'\right)^2 & \text{for } R'^2+Z'^2<1 \\ (R')^2\left[\frac{1}{2}+\frac{1}{(R'^2+Z'^2)^{3/2}}\right]^2 + \gamma(Z')^2\left[1-\frac{1}{(R'^2+Z'^2)^{3/2}}\right]^2 & \text{for } Z'^2+R'^2>1. \end{cases} \tag{A5}$$

Here, the scaled coordinates are given by $R' \equiv R/r_p$ and $Z' = Z/R_p$ and $\beta=(\alpha_z/\alpha_\perp)(1-\alpha_\perp B^2/MC^2)$.

[1] M. Amoretti, C. Amsler, G. Bonomi *et al.*, Nature (London) **419**, 456 (2002).
[2] G. Gabrielse, N. S. Bowden, P. Oxley *et al.*, Phys. Rev. Lett. **89**, 213401

(2002).
[3]G. Gabrielse, N. S. Bowden, P. Oxley *et al.*, Phys. Rev. Lett. **89**, 233401 (2002).
[4]M. E. Glinsky and T. M. O'Neil, Phys. Fluids B **3**, 1279 (1991).
[5]S. G. Kuzmin, T. M. O'Neil, and M. E. Glinsky, Phys. Plasmas **11**, 2382 (2004).
[6]D. Vrinceanu, B. E. Granger, R. Parrott *et al.*, Phys. Rev. Lett. **92**, 133402 (2004).
[7]S. G. Kuzmin and T. M. O'Neil, Phys. Rev. Lett. **92**, 243401 (2004).
[8]J. E. Avron, I. W. Herbst, and B. Simon, Ann. Phys. (N.Y.) **114**, 431 (1978).
[9]S. Saini and D. Farrelly, Phys. Rev. A **36**, 3556 (1987).
[10]J. B. Delos, S. K. Knudson, and D. W. Noid, Phys. Rev. A **30**, 1208 (1984).
[11]L. D. Landau and E. M. Lifshtz, *Quantum Mechanics: Non-relativistic Theory* (Pergamon, New York, 1977), p. 461.
[12]J. B. Taylor, Phys. Fluids **7**, 767 (1964).
[13]D. H. E. Dubin and T. M. O'Neil, Rev. Mod. Phys. **71**, 87 (1999).
[14]J. R. Brewer, J. D. Prestage, J. J. Bollinger, W. M. Itano, D. J. Larson, and D. J. Wineland, Phys. Rev. A **38**, 859 (1988).
[15]G. Gabrielse, A. Speck, C. H. Storry *et al.* Phys. Rev. Lett. **93**, 073401 (2004).